6-13-2014

Independent Evaluation of the SNODAS Snow Depth Product Using Regional Scale Lidar-Derived Measurements

A. R. Hedrick
Boise State University

H. P. Marshall
Boise State University

A. Winstral
USDA - ARS Northwest Watershed Research Center

K. Elder
USDA Forest Service

S. Yueh
California Institute of Technology

See next page for additional authors

The Cryosphere Discuss., 8, 3141–3170, 2014
www.the-cryosphere-discuss.net/8/3141/2014/
doi:10.5194/tcd-8-3141-2014

The Cryosphere Discussions
Open Access

Independent evaluation of the SNODAS snow depth product using regional scale LiDAR-derived measurements

A. Hedrick[1,2], H.-P. Marshall[1], A. Winstral[2], K. Elder[3], S. Yueh[4], and D. Cline[5]

[1]Boise State University, Center for the Geophysical Investigation of the Shallow Subsurface, Boise, Idaho 83725, USA
[2]USDA-ARS Northwest Watershed Research Center, 800 Park Blvd., Suite 105, Boise, Idaho 83712, USA
[3]USDA Forest Service, Rocky Mountain Research Station, Fort Collins, Colorado 80526, USA
[4]Jet Propulsion Laboratory, California Institute of Technology, Pasadena, California 91125, USA
[5]NOAA-NWS, Hydrology Laboratory, Office of Hydrologic Development, Silver Spring, Maryland 20910, USA

Received: 15 May 2014 – Accepted: 22 May 2014 – Published: 13 June 2014

Correspondence to: A. Hedrick (andrewhedrick@boisestate.edu)

Published by Copernicus Publications on behalf of the European Geosciences Union.

Abstract

Repeated Light Detection and Ranging (LiDAR) surveys are quickly becoming the de facto method for measuring spatial variability of montane snowpacks at high resolution. This study examines the potential of a 750 km^2 LiDAR-derived dataset of snow depths, collected during the 2007 northern Colorado Cold Lands Processes Experiment (CLPX-2), as a validation source for an operational hydrologic snow model. The SNOw Data Assimilation System (SNODAS) model framework, operated by the US National Weather Service, combines a physically-based energy-and-mass-balance snow model with satellite, airborne and automated ground-based observations to provide daily estimates of snowpack properties at nominally 1 km resolution over the coterminous United States. Independent validation data is scarce due to the assimilating nature of SNODAS, compelling the need for an independent validation dataset with substantial geographic coverage.

Within twelve distinctive 500 m × 500 m study areas located throughout the survey swath, ground crews performed approximately 600 manual snow depth measurements during each of the CLPX-2 LiDAR acquisitions. This supplied a dataset for constraining the uncertainty of upscaled LiDAR estimates of snow depth at the 1 km SNODAS resolution, resulting in a root-mean-square difference of 13 cm. Upscaled LiDAR snow depths were then compared to the SNODAS-estimates over the entire study area for the dates of the LiDAR flights. The remotely-sensed snow depths provided a more spatially continuous comparison dataset and agreed more closely to the model estimates than that of the in situ measurements alone. Finally, the results revealed three distinct areas where the differences between LiDAR observations and SNODAS estimates were most drastic, suggesting natural processes specific to these regions as causal influences on model uncertainty.

1 Introduction

Meltwater from mountain snowpacks is an important ecological component of Earth's water cycle. However, quantifying the amount of water stored in a snowpack from year to year remains difficult. Millions of people in the western United States rely on water that descends from the Rocky Mountains, where over 70 % of the annual water supply is delivered from melting snow (Carroll et al., 2006). Hydrologic models provide important information that assist water managers in mitigating flood disasters and water shortages each year.

The primary goal of most hydrologic snow models is to provide estimates of snow water equivalent, or SWE, over large mountain regions, but in addition most models include routines to estimate secondary snow properties. The methods used to estimate snowpack characteristics such as depth and density vary between models; some use empirical methods from available historical data, while others are more physics-based. Even so, SWE is but a function of depth and density, and if validation is achieved for either of these so-called secondary model components, then higher confidence can be placed into corresponding SWE estimates. Since snow depth varies considerably more than bulk density over space (Sturm et al., 2010) and is also inherently easier to measure, this study purports to examine the snow depth prediction component of a gridded, spatially-distributed snow model.

Due to the resolution capability and gridded nature of most distributed snow models, many small-scale features that affect spatial variability are either averaged or not considered, influencing the bulk estimates of total SWE and overall depth in each grid cell (Marchand and Killingtveit, 2005). Nevertheless, sub-grid spatial properties have been shown to have a significant effect on the accuracy of spatially distributed snow models (Luce et al., 1999; Liston, 2004; Skaugen and Randen, 2013), but the datasets required for parameter estimation and optimization are small and spatially sparse in mountain, tundra and shrubland environments (Elder et al., 1991; Sturm et al., 2001a, b; Hiemstra et al., 2002; Liston and Sturm, 2002; Schirmer and Lehning, 2011). Considerable

variability in the spatial snow distribution can be introduced through the interaction between wind and snow with terrain and vegetation (Elder et al., 1991; Blöschl, 1999; Liston et al., 2007). In fact, wind has been shown to be the dominant influence on spatial variability of snow in complex terrain (Pomeroy et al., 1993; Winstral et al., 2002; Sturm and Wagner, 2010). Without prior knowledge of the spatial snow distribution in a given area, arbitrary manual snow measurements will not provide accurate estimates of snow depth in alpine regions (Elder et al., 1991; Anderton et al., 2004; Erickson et al., 2005).

Various studies have shown that LiDAR (Light Detection and Ranging) surveys can provide spatial information on mountain snow depths at high-resolution over large areal extents that comprise various physiographic regimes (Hopkinson et al., 2004; Deems et al., 2006; McCreight et al., 2012). The first Cold Lands Processes Experiment (CLPX-1) of 2002–2003 in the Colorado Rocky Mountains, was the first large-scale coordinated study to use LiDAR acquisitions for the assessment of snow properties over a range of areas (Cline et al., 2009). Since then, numerous campaigns have used LiDAR to quantify spatial variability of snow depths in mountain terrain. Deems et al. (2006) used fractal analysis of the CLPX-1 LiDAR snow depths to determine scale-breaks, while Trujillo et al. (2007) found that spatial distributions of snow depth are strongly controlled by both wind redistribution and vegetation interception of snow over uneven surface topography in five of the CLPX-1 intensive study areas. More recently, LiDAR has been used with simple statistical models to determine scale invariance due to vegetation and wind direction (Trujillo et al., 2009) as well as to verify high-resolution dynamical snow models (Mott et al., 2011).

Even though depths can vary greatly over space in a snow pack, the overall distribution of snow has been found to exhibit spatial similarities from year to year (Hiemstra et al., 2006; Sturm and Wagner, 2010; Winstral and Marks, 2014). Repeated LiDAR surveys throughout single seasons (Schirmer and Lehning, 2011; Schirmer et al., 2011) and over multiple seasons (Deems et al., 2008) have found similar results through fractal analyses of the snow depth distributions. By comparing findings

from large-scale LiDAR snow depth surveys to operational hydrologic models, we can pinpoint causes of any shortcomings and subsequently refine model results.

Developed by the National Operational Hydrologic Remote Sensing Center (NOHRSC) and first operationally implemented in 2004, the Snow Data Assimilation System (SNODAS) estimates various snow properties by merging satellite, airborne, and ground-based snow data with modeled approximations of snow cover (Barrett, 2003). Historical model output from SNODAS is stored and archived at the National Snow and Ice Data Center (NSIDC) in Boulder, Colorado for every day that the model has been executed since its inception. These eight snow properties are the primary estimates that are made available to the public:

1. Snow water equivalent (SWE)
2. Snow depth
3. Snow melt runoff from the base of the snowpack
4. Sublimation from the snowpack
5. Sublimation of blowing snow
6. Solid precipitation
7. Liquid precipitation
8. Snowpack average temperature

A large portion of model fidelity is directed towards SWE prediction rather than any of the other model outputs because the amount of total water storage within snowpacks is far more important for water managers. The physically-based energy- and mass-balance NOHRSC Snow Model (NSM), described by Carroll et al. (2006), is the primary component of SNODAS, while an assimilation step gives analysts the ability

to decide every day whether to augment the model estimates with any available remote sensing or ground-based measurements. Ultimately, the final model product has a spatial resolution of approximately 1 km^2 over the coterminous United States.

Independent validation data for SNODAS is scarce as a consequence of the framework's data assimilating nature which ensures that all available data at the model scale (i.e. 1 km^2) is used to adjust estimates of the NSM (Barrett, 2003). An alternative validation method has been to perform comparisons of SNODAS with other hydrologic models and satellite remote sensing products. Rutter et al. (2008) compared various NSM properties with two energy-balance snow models, but found difficulty in constraining model uncertainties due primarily to the high sub-grid spatial variability exhibited in mountain snowpacks. Other studies have used SNODAS as the validation source for large-scale hydrologic models such as the Noah land surface model (Barlage et al., 2010), and SWE retrieval using satellite-based microwave radar remote-sensing platforms (Azar et al., 2008).

To our knowledge, only two validation studies of SNODAS' performance have been conducted using independent datasets and each of those studies relied on extensive in situ measurement campaigns. Clow et al. (2012) performed snow surveys of snow depth within 45 SNODAS pixels over a three month period in 2007. The results revealed that SNODAS performed satisfactorily for predicting snow depth in forested areas, but depth estimates in alpine areas were poor in comparison to manual measurements chiefly due to sub-grid scale variability from wind redistribution of snow. This discrepancy was addressed by applying a correction factor to account for wind redistribution of snow in the wind-affected alpine areas. In another study, Anderson (2011) intensively sampled three SNODAS pixels in the mountains just north of Boise, Idaho over the course of two winter seasons and found that SNODAS slightly under predicted snow depths in heavily-forested areas but maintained reasonable estimates of SWE overall. Each of the studies required an enormous amount of manpower and time to obtain the independent datasets for proper comparison, but came to somewhat differ-

ent conclusions about the model performance most likely due to the individual locations of the collected data (Idaho and Colorado, USA).

As the technology has become more widespread over the last decade, LiDAR for snow research has become increasingly popular. The advantages of LiDAR for spatially characterizing snow depths over large remote areas are finally being used to assess lower resolution hydro-meteorologic snow models. Melvold and Skaugen (2013) used six parallel 500 m × 80 km LiDAR surveys, each separated by 10 km, to investigate the Norwegian operational temperature index snow model, *seNorge*. After upscaling the LiDAR-derived 2 m resolution snow depths to the spatial resolution of the 1 km^2 gridded model output, the modeled results were found to accurately represent the remote sensing estimates despite the lack of sub-grid spatial information within the model structure.

To our knowledge, this study for the first time examines the performance of a physically-based hydro-meteorologic snow model in complex terrain using airborne LiDAR-derived snow depths that have been subjected to ground validation error analysis.

2 Study area

The second Cold Lands Processes Experiment campaign (CLPX-2, 2006–2008) was a multi-faceted mission designed to cover a much larger coincident extent than the previous campaign (CLPX-1, 2002–2003) three years prior. The primary objective of CLPX-2 was to acquire snow volume backscatter measurements from NASA's POLSCAT (POLarimetric SCATterometer) airborne Ku-band radar system and the necessary ground truth measurements (Yueh et al., 2009) for validation of the proposed NASA Snow and Cold Land Proceses (SCLP) and ESA Cold Regions Hydrology High-resolution Observatory (CoreH_2O) satellite missions (Rott et al., 2010). The airborne LiDAR portion of the campaign was intended to be an ancillary validation dataset for the radar measurements.

Three Intensive Observation Periods (IOPs) were organizeded over a 9 km × 84 km rectangular swath to the south and east of the town of Steamboat Springs in northern Colorado, USA (Fig. 1). During both IOP-1 (early December 2006) and IOP-3 (late February 2007), airborne LiDAR surveys were performed to provide high-resolution surface elevation change datasets to aid in the POLSCAT validation process. Covering approximately 750 km^2, the study area encompasses a wide range of elevations, terrain and vegetation types, and ecological classes. Maximum LiDAR-derived changes in snow depth varied from merely 30 cm in the central wind-swept prairies to over 4 m in the drifts of the higher elevations.

The study area can be viewed as containing three main classification areas: (1) the grass-covered, low-elevation rolling farmland in the Yampa River Valley in the far west; (2) the coniferous forests of the Rabbit Ears Pass portion of the Park Range as well as the foothills of the Medicine Bow Mountains in the far east; and (3) the sagebrush-dominated high desert of the central North Park region. Six SNOw TELemetry (SNOTEL) sites, operated by the National Resources Conservation Service (NRCS), are located within 15 km of the study area and yield a relatively dense network of automated measurements of various snowpack properties. The data from these ground-based measurement stations are often assimilated by SNODAS in order to augment the NSM estimates.

3 Methods

3.1 LiDAR acquisitions

Due to the supportive role of the LiDAR surveys, only two flights were planned and carried out concurrent with the POLSCAT radar acquisitions. On 3 December 2006 and 22 February 2007 LiDAR acquisitions were obtained by Fugro Horizons, Inc. using a Leica ALS50 laser range finder onboard a Cessna 310 aircraft flying at 10 000 feet a.g.l. The 1064 nm laser wavelength is the most commonly used for snow covered

surfaces owing to the minimal penetration depth on the order of only 1 cm (Deems et al., 2006). The pulse rate of 32 500 Hz, combined with the aircraft's speed, altitude, and scan rate, resulted in raw point clouds with nominal point spacings of 2.0–2.5 m, depending on surface roughness, canopy coverage and scan angle relative to the aircraft.

The LiDAR vendor filtered vegetation returns from ground returns using a minimum block mean algorithm and proprietary software to create vegetation-filtered point clouds for each flight with updated nominal point spacings of 2.5–3.0 m, again depending on the terrain, canopy cover and scan angle. Various alternative filtering algorithms were explored during the course of this study, but the decision was ultimately made to utilize the vendor-filtered data in order to maintain consistency over the large variety of landscapes. Next, we applied the open-source Points2Grid interpolation tool, employing an inverse distance weighting scheme, to produce a 5 m Digital Surface Model (DSM) for both of the vegetation-filtered point clouds. Because the CLPX-2 LiDAR scans were never acquired over an absolutely snow-free surface, as many of the higher elevations had already received snow by 3 December, the interpolated surfaces were differenced to provide a raster of the estimated change in total snow height between 3 December and 22 February at 5 m resolution (Fig. 1). This 5 m gridded product of LiDAR-estimated changes in snow depth will hereafter be referred to as L_{Est}. Though less dense than the original CLPX-1 acquisitions, the CLPX-2 LiDAR footprint covered many more terrain, vegetation, and snowpack classes, thereby providing a useful comparison tool for hydrologic snow models over large spatial extents.

3.2 In situ measurements

All remote sensing methods are subject to an appreciable amount of measurement uncertainty which should be quantified by ground validation if possible. Originally intended as the primary ground truth dataset for each POLSCAT radar acquisition over the 2006–2007 winter season (Yueh et al., 2009), the CLPX-2 intensive manual measurement campaign was arranged and completed by a team of 12–15 researchers

during each IOP. Twelve 500 m × 500 m "hourglass" transects, henceforth referred to as HG sites with each comprised of 47–50 evenly spaced snow depth measurements, were manually sampled during IOP-1 and IOP-3 within a day of each of the CLPX-2 LiDAR acquisitions (Fig. 1). The HG sites were chosen to represent physiographically distinctive regions of the CLPX-2 survey swath. Ground crews made measurements at preprogrammed waypoints loaded onto mapping grade handheld GPS units in order to maintain location consistency for each survey. We estimate the resulting relative point-to-point horizontal uncertainty between the HG surveys to be less than 2 m while the HG transect locations themselves can be approximated to 7 m accuracy in absolute space. The repeated HG depth measurements were differenced to provide a similar comparison metric of snow depth change to the L_{Est} dataset.

3.3 SNODAS snow depths

SNODAS estimates of snow depth were downloaded from the NSIDC for the two dates of the CLPX-2 LiDAR acquisitions (3 December 2006 and 22 February 2007), then spatially referenced to the UTM coordinate projection. The two rasters of snow depth were differenced to provide 1 km gridded model estimates of snow depth change, hereafter referred to as M_{Est}. Figure 2 depicts M_{Est} over the area surrounding the LiDAR swath, along with the locations of all nearby SNOTEL stations that can be used for model assimilation. In view of the fact that snow was already present over much of the study area on 3 December, it is paramount that no snow melt occurred between the survey dates in order to properly assess the snow depth component of SNODAS using LiDAR estimates alone. Therefore, we examined the SNODAS estimates of snow melt due to incoming solar radiation and sublimation (Fig. 3) and the six nearby SNOTEL stations to determine whether the LiDAR estimates of snow depth change are a viable comparison tool for SNODAS. As can be seen in Fig. 3, only in the North Park region did any appreciable melt occur (10–20 % of the total snow precipitation), while everywhere else experienced negligible snow melt, thus permitting further investigation of M_{Est}.

3.4 SNODAS/in situ measurement comparison

To provide a link to the previous ground-based SNODAS validation studies, we examined the ability of manual measurements from the twelve HG sites to represent model estimates of snow height change. Mentioned previously, Clow et al. (2012) averaged depth measurements from snow surveys carried out within 45 individual SNODAS pixels to perform model validation. We employed the same method to assess SNODAS-predicted snow depth changes using the CLPX-2 in situ HG transects. The mean change in snow depth at each HG site was found with an associated interquartile range, similar to the method used by Clow et al. (2012). Then, a coincident 1 km^2 SNODAS estimate of depth change was constructed over each HG transect site from the areal coverage fraction of the overlapping model pixels, creating an area-weighted average of M_{Est} centered over each HG measurement site. This spatial averaging was performed because the CLPX-2 campaign was not designed during the planning phase to be a validation source for SNODAS and the HG transects were therefore not aligned within individual model pixels.

3.5 Characterizing LiDAR uncertainty

The 750 km^2 CLPX-2 LiDAR dataset (L_{Est}) overlaps 980 individual SNODAS pixels completely[1], supplying a statistically robust dataset for determining contributing factors to model uncertainty. However, LiDAR measurements are fundamentally estimates themselves and require uncertainty assessments, which was available from the HG in situ measurements. To account for the horizontal position uncertainty in both the HG and L_{Est} datasets, the 5 m gridded L_{Est} snow depth changes were averaged in a 10 m

[1]Though previously stated as nominally 1 km^2, the actual resolution of SNODAS is 30 arcseconds because the model is implemented in the geographic coordinate system (Barrett, 2003). At the latitude of CLPX-2, that is equivalent to approximately 0.83 km^2.

radius around each reported in situ measurement location and treated as a separate point measurement for comparison purposes.

To perform the model comparison, the L_{Est} 5 m snow depth changes were binned into the spatial extents of the 980 overlaid SNODAS M_{Est} grid cells. Statistics were calculated within each 1 km pixel, resulting in a mean, standard deviation, and interquartile range of LiDAR-estimated snow depth change over the CLPX-2 study area at the SNODAS model resolution. The mean L_{Est} snow depth changes are portrayed in Fig. 4.

4 Results and discussion

We examined how well the twelve averaged HG measurement transects were able to substantiate the SNODAS estimates of snow depth change. Figure 5a shows the relationship between M_{Est} and the mean manually-measured changes in snow depth at each of the HG sites, while Fig. 5b shows the difference between the HG in situ measurements and M_{Est} as a function of the mean HG measurements themselves. The trend of this limited dataset suggests that as the mean snow depth within a model pixel increases above approximately 40 cm, the ability of SNODAS to estimate the amount of total snow depth change decreases substantially. Also, it is not clear from the small sample size of the in situ data what physical factors could be influencing such discrepancies and a much more spatially extensive dataset, such as the CLPX-2 LiDAR, is required for determining the underlying causes of model error.

The exhaustive CLPX-2 in situ HG measurement campaign provided an ideal dataset for limiting uncertainty in the large-scale LiDAR surveys of 3 December 2006 and 22 February 2007. The changes in snow depth as measured by the standard probing method and interpolated from the LiDAR surveys were compared throughout all twelve HG sites individually, and then averaged on a site by site basis (Fig. 6), again similar to the averaging scheme used by Clow et al. (2012). In this instance, the RMS difference of 12.9 cm between mean HG and mean L_{Est} snow depth changes for all twelve CLPX-2 HG site locations is well within the bounds of conventional airborne

LiDAR uncertainty estimates (Baltsavias, 1999; Hodgson and Bresnahan, 2004). Also, the averaged HG measurements and L_{Est} observations are highly correlated with a linear r-squared coefficient of 0.942. It can be seen in Fig. 6 that the mean L_{Est} snow depth change consistently underestimates the mean HG measurements by 5–30 cm, with deeper snowpacks tending to be more sensitive to higher spatial variability and in situ under sampling.

A variety of factors likely attribute to the underestimates by the LiDAR-derived snow depth change when compared to the HG point measurements. One viable explanation would be the difference in measurement support between LiDAR and in situ measurements. While the manual depth measurement support was less than one centimeter (the size of the depth probe tip), the LiDAR-derived snow depth change was averaged over all the 5 m pixels within a 10 m radius of the reported in situ measurement location. This smoothing of the snow height change could result in lower reported values than that of the point measurement when scale breaks in snow depth are present that are lower than the LiDAR-averaged areal extent. Even so, the correlation between the ground-based and airborne data shows that we should be able to trust the 1 km spatially-averaged, LiDAR-derived estimates of snow depth change within a range of approximately ±13 cm.

The comparison between M_{Est} and mean L_{Est} snow depth change within the model pixels (Fig. 7) determined an $r^2 = 0.72$, signifying a reasonably strong correlation between the two estimate datasets. Since snow melt between the LiDAR flights was found to be an insignificant portion of the snowpack evolution (Fig. 3), the actual changes in snow depth over the study area were primarily influenced by accumulation, densification, and redistribution factors (sublimation effects are beyond the scope of this paper).

To investigate the primary cause of disagreement between M_{Est} and L_{Est}, seven potential physiographic parameters were culled from the LiDAR data to perform a regression analysis. In addition to the LiDAR-derived snow depth changes and the vegetation-filtered elevations, vegetation height and canopy coverage across the survey swath was calculated at 5 m resolution using both the raw and vegetation-filtered December

LiDAR point returns. Vegetation heights and elevations were each upscaled to the 1 km SNODAS resolution in a similar fashion to the LiDAR snow depth change, while the vegetation density was calculated by finding the number of 5 m pixels within each 1 km SNODAS grid cell that contained LiDAR first returns greater than 50 cm above the filtered surface. Lastly, the interquartile range of the 1 km averaged (upscaled) variables was determined to result in a group of 7 individual predictor variables for regression analysis.

1. Vegetation density [%]
2. Mean vegetation height [cm]
3. Inter-quartile range of vegetation height [cm]
4. Mean snow depth change [cm] (3 December–22 February)
5. Inter-quartile range of snow depth change [cm]
6. Mean elevation [m]
7. Inter-quartile range of elevation [m]

The upscaled snow depth changes were overwhelmingly found to best predict the discrepancy between M_{Est} and L_{Est}, indicating that none of the other six factors singularly influenced SNODAS performance over the study area. Figure 8 shows the plot of mean L_{Est} snow depth changes against the $M_{\mathrm{Est}} - L_{\mathrm{Est}}$ differences within each model pixel. Within that plot, the pink vertical and blue horizontal stripes between −13 and +13 cm on each axis represent the minimum attainable resolution of the LiDAR-derived snow depth values determined from the HG ground-based measurement data. Three regions have been circled in the figure, each corresponding to portions of the difference dataset that were found to be outside the uncertainty levels of the LiDAR-derived changes in snow depth.

Contrasting the images of $M_{Est} - L_{Est}$ (Fig. 9) and mean L_{Est} (Fig. 4) reveals the geographic locations of the three regions within the survey swath containing the greatest SNODAS and LiDAR disagreements. Within these three regions specific physiographic factors are likely the cause of greater relative discrepancy.

Region #1: North Park

The region with the lowest annual snow totals is comprised of pixels that SNODAS estimated to have a larger positive change in snow depth between LiDAR acquisitions. However, the LiDAR snow depth changes within these pixels are well below the trusted LiDAR uncertainty level (the pink vertical stripe). These pixels are located in the North Park region of the survey area, where the flat landscape is densely populated by low sagebrush ($\approx$ less than 30 cm) and high winds frequently scour the snow above and near the height of the sage throughout the winter. The snow that remains is subsequently packed between the low vegetation and the snow height changes very little throughout the year once it has reached a height similar to the sagebrush. SNODAS does incorporate a sublimation factor due to wind into the accumulation model, but the nearest SNOTEL station used in the assimilation step is located nearly 15 kilometers to the southwest in a much different landscape so wind speeds and directions are not well-represented in the area. The locations of the region #1 pixels are roughly delineated in Fig. 9.

Region #2: East slope of Rabbit Ears Pass

Pixels that comprise region #2 in Fig. 8 are where snow depths are similarly estimated by SNODAS to have changed more than observed by the LiDAR. However, the geographic location of the pixels are in a region with higher snow accumulation totals, which are above the lower LiDAR uncertainty level of 13 cm. Again delineated in Fig. 9, these pixels are nestled directly to the east of Rabbit Ears Pass where the Columbine SNOTEL station provides assimilation data for SNODAS. Since the relative error of

the LiDAR observations is small and a large altitudinal gradient can be seen in L_{Est} changes in snow depth (Fig. 4), this discrepancy can possibly be attributed to SNODAS over-distributing the SNOTEL information to areas of lower elevations and vegetation types. Future study on regions such as this would be important for determining optimal precipitation forcings by the SNODAS data assimilation process.

Region #3: Rabbit Ears Pass

Finally, the region #3 pixels represent an area where the upscaled LiDAR changes in snow depth are significantly larger than the SNODAS estimates. These pixels occur primarily in topographically complex areas with exceptionally high snow totals and dense coniferous forests, once again outlined in Fig. 9. The probable controlling factor of underestimation by SNODAS in this region is the sub-kilometer scale heterogeneity of snow distribution caused by both vegetation and topography. SNODAS has been found to underestimate snow depths in similar forested alpine terrain (Anderson, 2011), so this result is not unexpected.

5 Conclusions

Over the past decade, high resolution snow depth information has become a highly sought-after data product by snow researchers and many scientific questions have been addressed using the spatial continuity and extent provided by LiDAR surveys. This study first examined the ability of ground-based measurements to constrain remote sensing uncertainty, and in turn compared the remote sensing estimates to an operational hydrologic model for validation purposes. In this case, the CLPX-2 ground truth campaign was vitally important for quantifying uncertainty in the LiDAR snow depth estimates, revealing the necessity of similar campaigns to complement future LiDAR remote sensing missions.

From the comparison study, three distinct regions were extracted that exhibited greater disagreement than could be explained by LiDAR estimate uncertainty alone. Distinct physiographic characteristics within these three regions ultimately affected the accuracy of the SNODAS predictions of snow height change between the two LiDAR acquisitions.

To further investigate model performance, more studies are needed from subsequent LiDAR-derived snow depth datasets that focus on the performance of SNODAS as a function of the distance from SNOTEL stations. Additionally, micro-scale wind redistribution effects could be applied within the model structure to assist in areas where blowing snow transport is a major cause of spatial variability. Finally, large-scale coincident density surveys would allow model validation with LiDAR-derived snow depths as well as in situ estimates of SWE, for which SNODAS is likely to be more accurate than compared with depth alone.

Author contributions

Adam Winstral supplied modeling expertise, Kelly Elder produced the archived LiDAR datasets and orchestrated the in situ CLPX-2 measurement campaign, Simon Yueh and Donald Cline managed and coordinated the CLPX-2 campaign of 2006–2007, and Andrew Hedrick performed the validation comparison and manuscript preparation with significant support from Hans-Peter Marshall and contributions from all co-authors.

Acknowledgements. The authors would like to express their gratitude to all the researchers involved in the intensive ground-based measurement campaign during CLPX-2. The CLPX-2 LiDAR datasets were archived and maintained by Fugro Horizons, Inc. Daily SNODAS model runs from 2003 to the present day are archived at the National Snow and Ice Data Center in Boulder, Colorado. This research was funded in part by NASA grant #NNX10AO02G (NASA New Investigator Program) and NASA grant #NNX10AN30A (NASA EPSCoR Program).

References

Anderson, B. T.: Spatial Distribution and Evolution of a Seasonal Snowpack in Complex Terrain: an Evaluation of the SNODAS Modeling Product, Masters thesis, Boise State University, Boise, Idaho, United States, 2011. 3146, 3156

Anderton, S. P., White, S. M., and Alvera, B.: Evaluation of spatial variability in snow water equivalent for a high mountain catchment, Hydrol. Process., 18, 435–453, 2004. 3144

Azar, A. E., Ghedira, H., Romanov, P., Mahani, S., Tedesco, M., and Khanbilvardi, R.: Application of satellite microwave images in estimating snow water equivalent, J. Am. Water Resour. Assoc., 44, 1347–1363, 2008. 3146

Baltsavias, E.: Airborne laser scanning: basic relations and formulas, ISPRS J. Photogramm., 54, 199–214, 1999. 3153

Barlage, M., Chen, F., Tewari, M., Ikeda, K., Gochis, D., Dudhia, J., Rasmussen, R., Livneh, B., Ek, M., and Mitchell, K.: Noah land surface model modifications to improve snowpack prediction in the Colorado Rocky Mountains, J. Geophys. Res., 115, D22101, doi:10.1029/2009JD013470, 2010. 3146

Barrett, A. P.: National Operational Hydrologic Remote Sensing Center SNOw Data Assimilation System (SNODAS) Products at NSIDC, NSIDC Spec. Rep. 11, National Snow and Ice Data Center, Boulder, CO, USA, 2003. 3145, 3146, 3151

Blöschl, G.: Scaling issues in snow hydrology, Hydrol. Process., 13, 2149–2175, 1999. 3144

Carroll, T., Cline, D., Olheiser, C., Rost, A., Nilsson, A., Fall, F., Bovitz, C., and Li, L.: NOAA's national snow analyses, in: Proceedings, 74th Annu. Meet. West. Snow Conf., 1–14, Las Cruces, New Mexico, 17–20 April, 2006. 3143, 3145

Cline, D., Yueh, S., Chapman, B., Stankov, B., Gasiewski, A., Masters, D., Elder, K., Kelly, R., Painter, T. H., Miller, S., Katzberg, S., and Mahrt, L.: NASA Cold Land Processes Experiment (CLPX 2002/03): airborne remote sensing, J. Hydrometeorol., 10, 338–346, 2009. 3144

Clow, D. W., Nanus, L., Verdin, K. L., and Schmidt, J.: Evaluation of SNODAS snow depth and snow water equivalent estimates for the Colorado Rocky Mountains, USA, Hydrol. Process., 26, 2583–2591, 2012. 3146, 3151, 3152

Deems, J. S., Fassnacht, S. R., and Elder, K. J.: Fractal distribution of snow depth from lidar data, J. Hydrometeorol., 7, 285–297, 2006. 3144, 3149

Deems, J. S., Fassnacht, S. R., and Elder, K. J.: Interannual consistency in fractal snow depth patterns at two Colorado mountain sites, J. Hydrometeorol., 9, 977–988, 2008. 3144

Elder, K., Dozier, J., and Michaelsen, J.: Snow accumulation and distribution in an alpine watershed, Water Resour. Res., 27, 1541–1552, 1991. 3143, 3144

Erickson, T. A., Williams, M. W., and Winstral, A.: Persistence of topographic controls on the spatial distribution of snow in rugged mountain terrain, Colorado, United States, Water Resour. Res., 41, 1–17, 2005. 3144

Hiemstra, C. A., Liston, G. E., and Reiners, W. A.: Snow redistribution by wind and interactions with vegetation at upper treeline in the Medicine Bow Mountains, Wyoming, USA, Arctic, Antarct. Alp. Res., 34, 262–273, 2002. 3143

Hiemstra, C. A., Liston, G. E., and Reiners, W. A.: Observing, modelling, and validating snow redistribution by wind in a Wyoming upper treeline landscape, Ecol. Model., 197, 35–51, 2006. 3144

Hodgson, M. E. and Bresnahan, P.: Accuracy of airborne lidar-derived elevation: empirical assessment and error budget, Photogramm. Eng. Remote Sens., 70, 331–339, 2004. 3153

Hopkinson, C., Sitar, M., Chasmer, L., and Treitz, P.: Mapping snowpack depth beneath forest canopies using airborne lidar, Photogramm. Eng. Remote Sens., 70, 323–330, 2004. 3144

Liston, G. E.: Representing subgrid snow cover heterogeneities in regional and global models, J. Climate, 17, 1381–1398, 2004. 3143

Liston, G. E. and Sturm, M.: Winter precipitation patterns in arctic alaska determined from a blowing-snow model and snow-depth observations, J. Hydrometeorol., 3, 646–660, 2002. 3143

Liston, G. E., Haehnel, R. B., Sturm, M., Hiemstra, C. A., Berezovskaya, S., and Tabler, R. D.: Simulating complex snow distributions in windy environments using SnowTran-3D, J. Glaciol., 53, 241–256, 2007. 3144

Luce, C. H., Tarboton, D. G., and Cooley, K. R.: Sub-grid parameterization of snow distribution for an energy and mass balance snow cover model, Hydrol. Process., 13, 1921–1933, 1999. 3143

Marchand, W. D. and Killingtveit, A.: Statistical probability distribution of snow depth at the model sub-grid cell spatial scale, Hydrol. Process., 19, 355–369, 2005. 3143

McCreight, J. L., Slater, A. G., Marshall, H. P., and Rajagopalan, B.: Inference and uncertainty of snow depth spatial distribution at the kilometre scale in the Colorado Rocky Mountains: the effects of sample size, random sampling, predictor quality, and validation procedures, Hydrol. Process., 28, 933–957, 2014. 3144

Melvold, K. and Skaugen, T.: Multiscale spatial variability of lidar-derived and modeled snow depth on Hardangervidda, Norway, Ann. Glaciol., 54, 273–281, 2013. 3147

Mott, R., Schirmer, M., and Lehning, M.: Scaling properties of wind and snow depth distribution in an Alpine catchment, J. Geophys. Res., 116, 1–8, 2011. 3144

Pomeroy, J., Gray, D., and Landine, P.: The prairie blowing snow model: characteristics, validation, operation, J. Hydrol., 144, 165–192, 1993. 3144

Rott, H., Yueh, S. H., Cline, D. W., Duguay, C., Essery, R., Haas, C., Heliere, F., Kern, M., Macelloni, G., Malnes, E., Nagler, T., Pulliainen, J., Rebhan, H., and Thompson, A.: Cold regions hydrology high-resolution observatory for snow and cold land processes, Proc. IEEE, 98, 752–765, 2010. 3147

Rutter, N., Cline, D., and Li, L.: Evaluation of the NOHRSC Snow Model (NSM) in a one-dimensional mode, J. Hydrometeorol., 9, 695–711, 2008. 3146

Schirmer, M. and Lehning, M.: Persistence in intra-annual snow depth distribution: 2. Fractal analysis of snow depth development, Water Resour. Res., 47, 1–14, 2011. 3143, 3144

Schirmer, M., Wirz, V., Clifton, A., and Lehning, M.: Persistence in intra-annual snow depth distribution: 1. Measurements and topographic control, Water Resour. Res., 47, 1–16, 2011. 3144

Skaugen, T. and Randen, F.: Modeling the spatial distribution of snow water equivalent, taking into account changes in snow-covered area, Ann. Glaciol., 54, 305–313, 2013. 3143

Sturm, M. and Wagner, A. M.: Using repeated patterns in snow distribution modeling: an Arctic example, Water Resour. Res., 46, 1–15, 2010. 3144

Sturm, M., Liston, G. E., Benson, C. S., and Holmgren, J.: Characteristics and growth of a snowdrift in Arctic Alaska, USA, Arctic, Antarct. Alp. Res., 33, 319–329, 2001a. 3143

Sturm, M., McFadden, J. P., Liston, G. E., Chapin III, F. S., Racine, C. H., and Holmgren, J.: Snow–shrub interactions in Arctic tundra: a hypothesis with climatic implications, J. Climate, 14, 336–345, 2001b. 3143

Sturm, M., Taras, B., Liston, G. E., Derksen, C., Jonas, T., and Lea, J.: Estimating snow water equivalent using snow depth data and climate classes, J. Hydrometeorol., 11, 1380–1394, 2010. 3143

Trujillo, E., Ramírez, J. A., and Elder, K. J.: Topographic, meteorologic, and canopy controls on the scaling characteristics of the spatial distribution of snow depth fields, Water Resour. Res., 43, 1–17, 2007. 3144

Trujillo, E., Ramirez, J. A., and Elder, K. J.: Scaling properties and spatial organization of snow depth fields in sub-alpine forest and alpine tundra, Hydrol. Process., 23, 1575–1590, 2009. 3144

Winstral, A. and Marks, D.: Long-term snow distribution observations in a mountain catchment: Assessing variability, time stability, and the representativeness of an index site, Water Resour. Res., 50, 293–305, 2014. 3144

Winstral, A., Elder, K., and Davis, R. E.: Spatial snow modeling of wind-redistributed snow using terrain-based parameters, J. Appl. Meteorol., 3, 524–539, 2002. 3144

Yueh, S. H., Dinardo, S. J., Akgiray, A., West, R., Cline, D. W., and Elder, K.: Airborne ku-band polarimetric radar remote sensing of terrestrial snow cover, IEEE T. Geosci. Remote, 47, 3347–3364, 2009. 3147, 3149

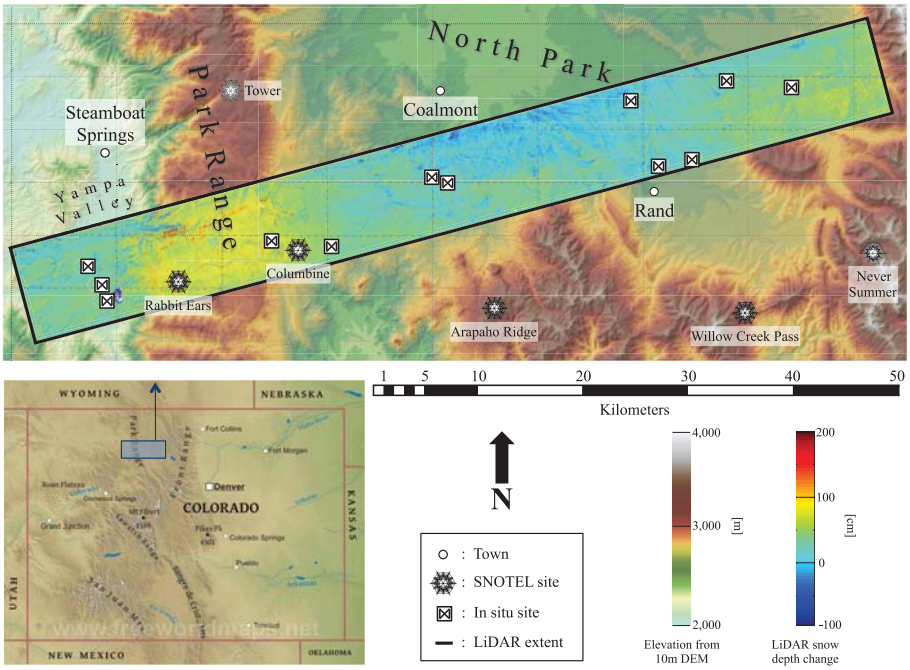

Figure 1. Location of the CLPX-2 LiDAR footprint in Colorado, USA. The 5 m, LiDAR-derived changes in snow depth between 3 December 2006 and 22 February 2007, overlaid upon a 10 m DEM with nearby towns, SNOTEL sites, and IOP in situ measurement locations indicated.

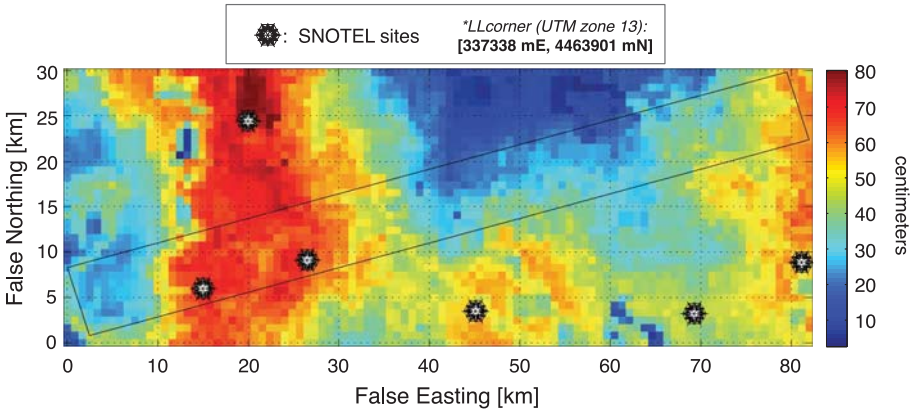

Figure 2. SNODAS estimates of snow depth change between 3 December 2006 and 22 February 2007. Depicted are the six nearest SNOTEL sites, used for data assimilation by SNODAS, and the CLPX-2 LiDAR footprint.

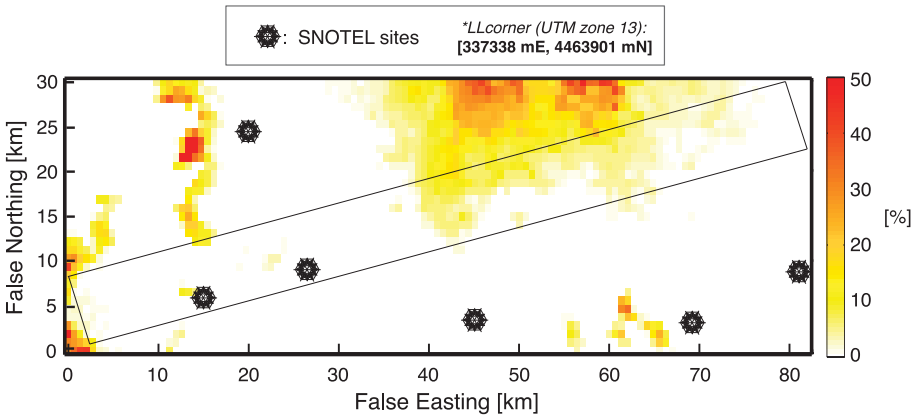

Figure 3. SNODAS estimates of snow melt as a percentage of the estimated mass lost from the estimated mass gained between 3 December 2006 and 22 February 2007.

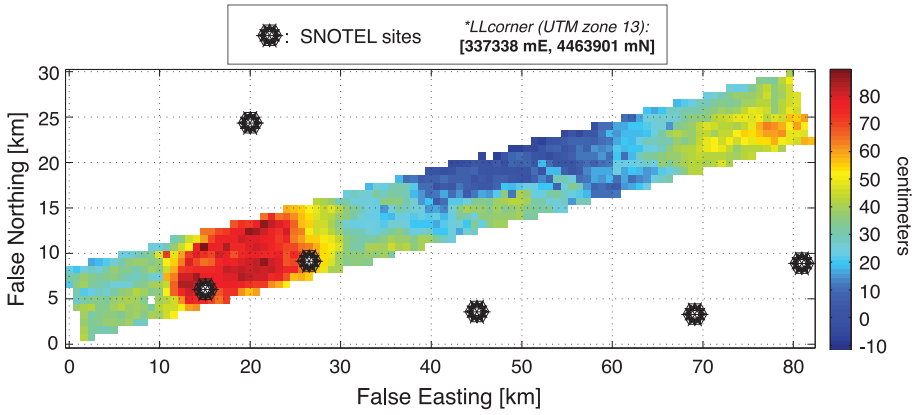

Figure 4. LiDAR-derived snow depth change between 3 December 2006 and 22 February 2007 upscaled by averaging to the resolution of SNODAS (1 km^2).

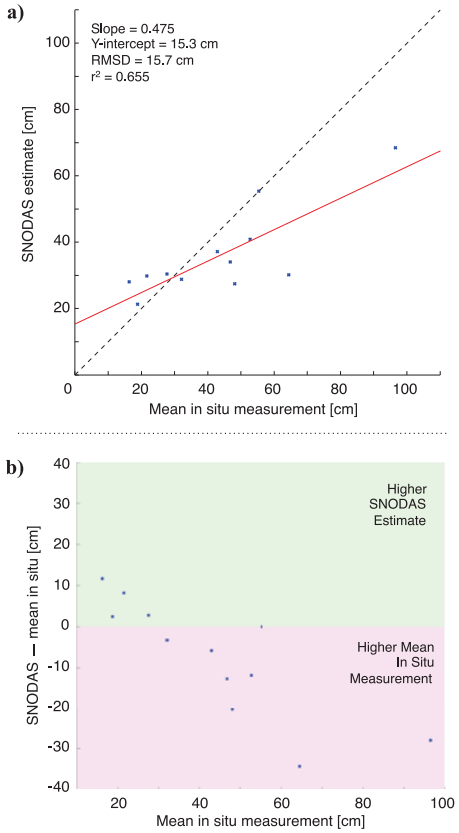

Figure 5. (a) shows the SNODAS estimate of snow depth change vs. the mean snow depth change from the CLPX-2 hglass (HG) in situ measurement sites. **(b)** displays the model-measurement difference (SNODAS estimate – mean in situ measurement) against the mean in situ measurements. For sites with higher snowfall totals, SNODAS tends to underestimate the change in snow depth.

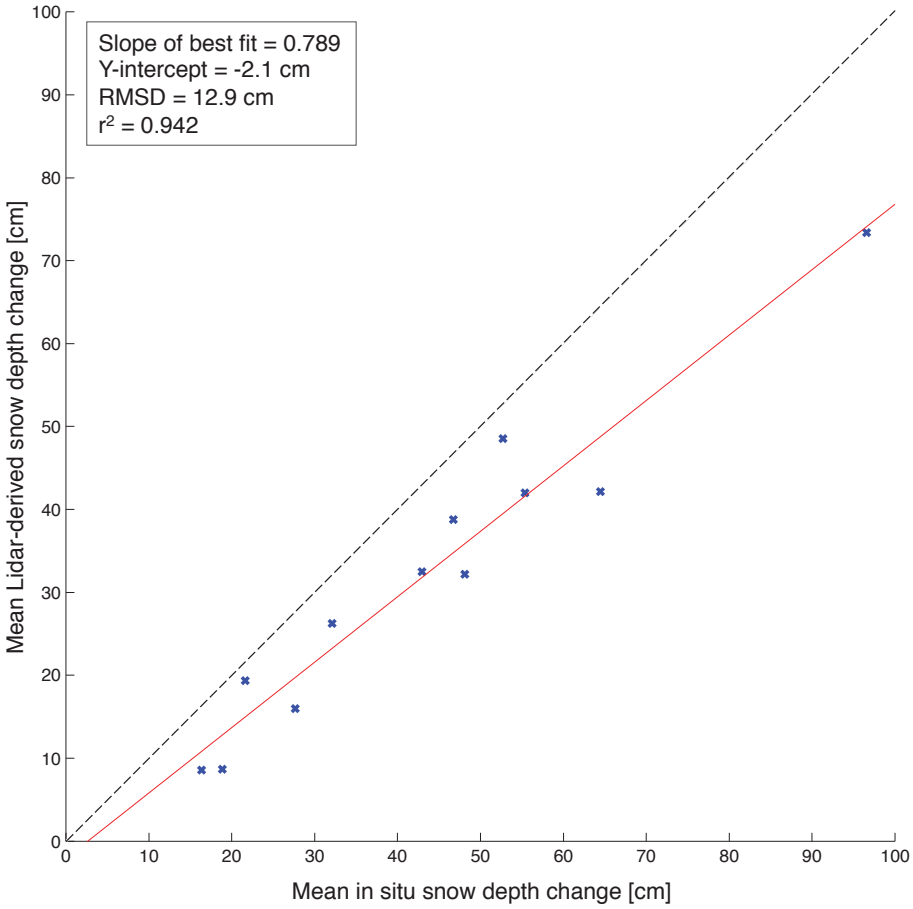

Figure 6. Scatter plot comparing the CLPX-2 mean in situ-measured and the LiDAR-derived change in snow depth between 3 December 2006 and 22 February 2007 over the twelve intensive observation hourglass sites.

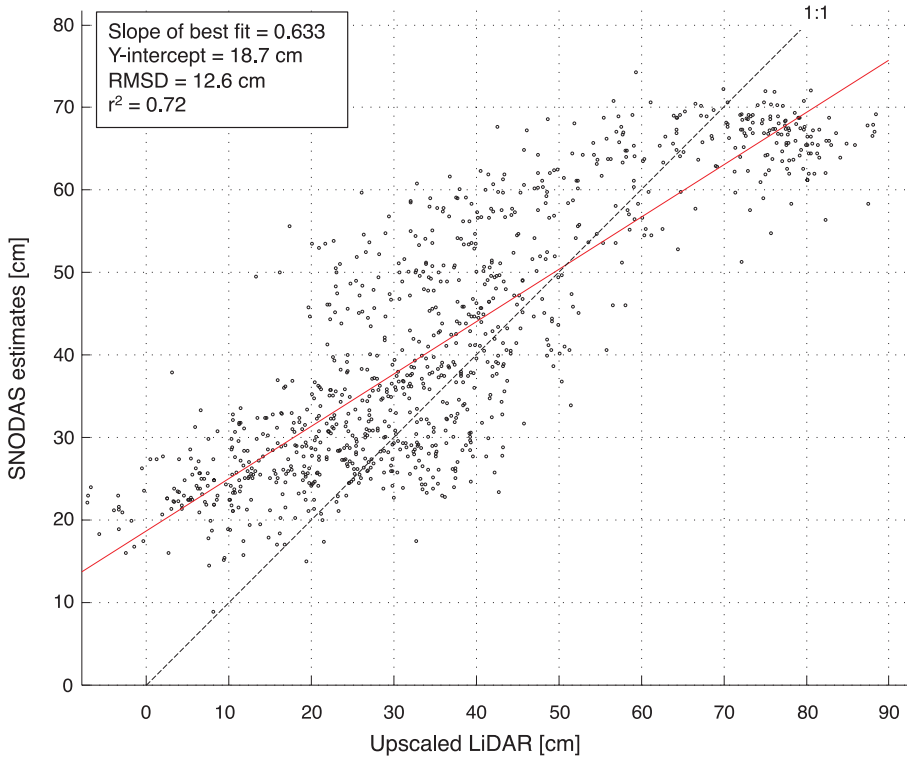

Figure 7. Model estimates plotted against mean LiDAR-derived snow depth change within all 1 km^2 SNODAS pixels (n = 980).

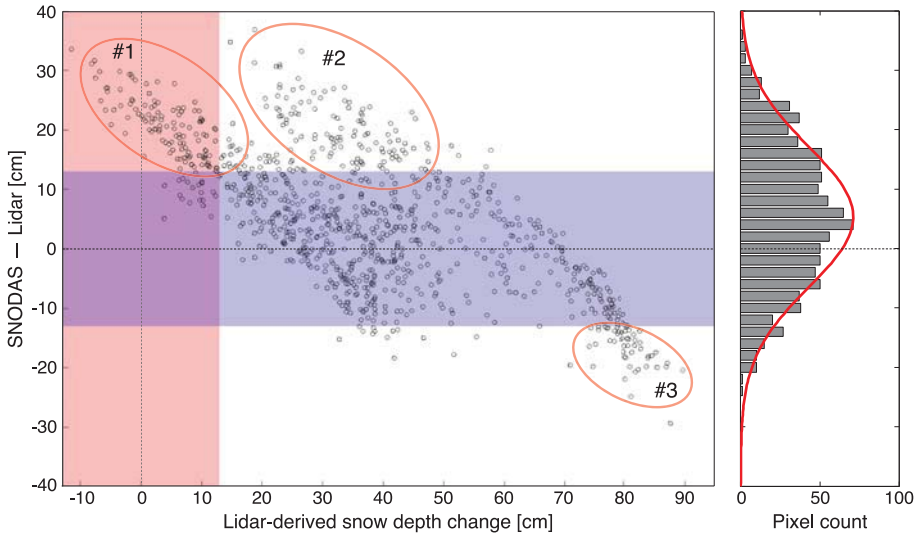

Figure 8. Pixel by pixel SNODAS-LiDAR differences of snow depth change plotted against the mean LiDAR depth change within each SNODAS pixel. The pink and blue shaded areas represent the ±13 cm error threshold for the upscaled LiDAR estimates determined from the CLPX-2 in situ measurements. Three distinct regions are circled that fall outside the 13 cm error threshold, signifying a particular physiographic forcing factor present in the three specific areas. Also plotted is a histogram of differences showing a bias toward higher SNODAS estimates over the CLPX-2 study area.

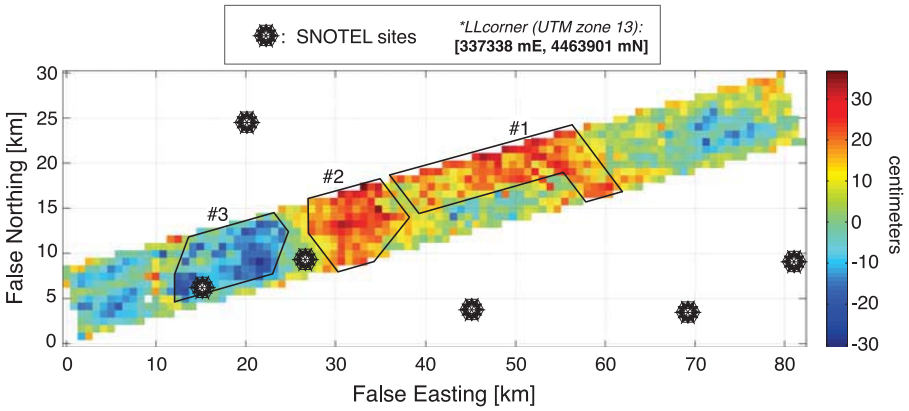

Figure 9. Image of the difference (SNODAS – LiDAR) between model and remote sensing estimates of snow depth change between 3 December 2006 and 22 February 2007 over the CLPX-2 study area. The three outlined regions correspond to the regions highlighted in Fig. 8.